ORIGINAL PAPER
Polish Journal of Microbiology
2025, Vol. 74, No 1, 19–32
https://doi.org/10.33073/pjm-2025-002

Optimization and Mechanism of Ca^{2+} Biosorption by *Virgibacillus pantothenticus* Isolated from Gelatine Wastewater

HAIWEI REN[1, 2], YUMENG XIANG[1], AILI ZHANG[1], HONGYUAN ZHAO[1]*, HUI TIAN[1, 2], XIAOPENG GUO[1], YI ZHENG[3] and BINGYUN ZHANG[1]

[1] School of Life Science and Engineering, Lanzhou University of Technology, Lanzhou, P. R. China
[2] China Northwest Collaborative Innovation Center of Low-carbon Urbanization Technologies of Gansu and MOE, Lanzhou, P. R. China
[3] Department of Grain Science and Industry, Kansas State University, Manhattan, United States

Submitted 6 October 2024, accepted 24 November 2024, published online 25 March 2025

Abstract

Gelatine-processing wastewater contains much residual sludge due to its high calcium ion concentration and chemical oxygen demand. In this study, N3-4, a microbial strain with excellent calcium tolerance capacity, was screened and identified as *Virgibacillus pantothenticus* using morphological observation, physiological and biochemical testing, and 16S rRNA sequence analysis. Its growth characteristics were investigated, and the maximum adsorption of calcium reached 572.43 μg/g under the optimal conditions (contact time, 72.68 min; biomass dosage, 1.3 g/l; initial calcium concentration, 142.01 mg/l). Conditions were optimized using response surface methodology and structural characterization. The structure of the bacterial pellets was altered from flat to rough, accompanied by bulges and sediments after Ca^{2+} treatment, according to structural characterization. Energy-dispersive X-ray spectroscopy of the bacterial precipitates under calcium(II) treatment revealed the immobilization of Ca^{2+} species on the bacterial cell surface. The results indicate that –OH, $-NH_2$, C≡C, C=O, $-CH_2$, –C–O–, and –C–N groups play a significant role in calcium dispersion on the surface of *V. pantothenticus*.

K e y w o r d s: *Virgibacillus pantothenticus*, biosorption, calcium dispersion, structural characterization, adsorption capacity

Introduction

Gelatine processing is one of the most polluting industries worldwide; one ton of processed gelatine can generate 1500 m^3 of wastewater, which is rich in calcium, nitrogen, and phosphorus (Awasthi et al. 2016; Wang et al. 2018; Tawfik et al. 2021). Although calcium is traditionally considered a non-toxic metal, high concentrations (> 5 g/l) can be severely toxic to living cells (Hansda et al. 2016; Wang et al. 2018). High calcium ion concentrations in wastewater can lead to catastrophic problems, such as pipe blockages and corrosion (Li et al. 2022). They can also affect biological treatment efficiency because calcium precipitates on granular sludge and reduces the biological activity of microorganisms (Liu et al. 2011).

Generally, heavy metals exist in insoluble forms that the body cannot absorb; however, those produced by anthropogenic sources are highly bioavailable because of their mobile, soluble active forms (Priya et al. 2022). The calcium concentration in gelatine wastewater polluted by acidification can reach 20 g/l, indicating that few microorganisms can survive sewage disposal in harmful environments (Wang et al. 2018). If untreated gelatine wastewater is discharged directly into receiving waters, serious environmental problems can occur. There is no cost-effective method for high-calcium wastewater pretreatment; it is usually transported directly into a biotreatment unit. Therefore, it is important to identify microorganisms with superior calcium resistance and calcium absorption abilities in wastewater.

To date, various chemical, physical, and biological technologies have been used to eliminate pollutants from wastewater (Elsayed et al. 2023), but these have limitations (Razzak et al. 2022). Traditional physical and chemical methods, such as neutralization, chemical precipitation, and coagulation, are inefficient and prone to secondary pollution and other problems. Other

* Corresponding author: Zhao H , School of Life Science and Engineering, Lanzhou University of Technology, Gansu Province, Lanzhou, P. R. China; **e-mail: 20230064@lut.edu.cn**

adsorption or ion exchange methods are effective for low-concentration heavy metal wastewater but are uneconomical and have low metal resource recovery values (Shi et al. 2023). Sodium addition can effectively promote calcium ion precipitation by generating calcium carbonate sediment. This method introduces sodium ions into the wastewater, leading to detrimental environmental effects. It is crucial to develop cost-effective, efficient, and environmentally friendly techniques for effectively removing calcium ions from gelatin-processing wastewater (Xu et al. 2017).

Biosorption is a simple, low-cost, and environmentally friendly wastewater treatment process (Razzak et al. 2022; Karnwal 2024). Its advantages over traditional treatment methods include low cost, less chemical and biological sludge, no demand for extra nutrients, high removal efficiency for less concentrated solutions, and biosorbent regeneration and metal recovery (Jiao et al. 2024).

According to previous studies, most metals adsorbed by microorganisms are copper, lead, cadmium, and nickel, but not calcium (He et al. 2022). Unlike other toxic heavy metals, biosorption rarely eliminates calcium, even though calcium-ion-rich wastewater must be treated urgently.

This study screened the calcium-tolerant microbial strain N3-4 from gelatine-processing wastewater, followed by morphological observation, physiological and biochemical tests, and 16S rRNA sequence analysis. Its growth characteristics were also investigated. Its growth characteristics were also investigated. The optimal adsorption conditions for strain N3-4 in gelatine wastewater were determined using a unidirectional test and response surface methodology (RSM), to provide theoretical references for the remediation of high-calcium-containing water pollution.

Experimental

Materials and Methods

Bacterial strain and chemical reagents. Calcium-tolerant strain N3-4 was previously isolated from gelatine wastewater at Amin Biological Gelatin Co. (Gansu, China). The solid medium contained 3 g beef paste, 10 g peptone, and 5 g NaCl dissolved in 1,000 ml distilled water at a final pH of 7.4.

Identification of N3-4. ***Morphological identification.*** After plate culture, the colonies' shape, size, color, concentration, transparency, margins, and elevation on the medium were observed under a light microscope.

Physiological and biochemical identification. Physiological and biochemical identification of the strain was carried out according to the "Manual of Identification of Common Bacterial Systems", "Berger's Manual of Bacteriological Identification", and "Common Identification Methods of General Bacteria".

16S rRNA identification. Bacterial 16S rRNA was amplified by PCR (27F: 5'-AGAGTTTGATCCTGGC TCAG-3', 1492R: 5'-GGTTACCTTGTTACGACTT-3'). The 16S rRNA amplified fragments were detected by agarose electrophoresis and the PCR amplified products were sent for sequencing at Lanzhou Tianqi Gene Biotechnology Co., Ltd (China). The 16S rRNA sequences were uploaded to the NCBI database, and the strain was analyzed and compared with the known 16S rRNA sequences in GenBank using BLAST. A phylogenetic tree was constructed using MEGA 5.0 (Sedlakova-Kadukova et al. 2019). The 16S rRNA gene sequence of N3-4 was deposited in GenBank under the accession number OP895700.

Growth curve determination. Strains were picked and inoculated in 30 ml beef paste peptone liquid medium, incubated at 37°C and 120 rpm for 18 h, and then connected to sterilized conical flasks containing 30 ml beef paste peptone liquid medium at 5% inoculum. The culture was incubated at 37°C and 120 rpm on a shaker with constant temperature oscillation using a time gradient (0, 3, 6, 9, 12 h). Next, 4 ml bacterial solution was aspirated from the conical flask with a pipette on a sterile bench, and the OD_{600} values of the bacterial suspensions at different incubation times were determined using a UV spectrophotometer.

Single factor testing of Ca^{2+} biosorption. The optimum biosorption conditions for strain N3-4 were preliminarily identified using one-way experiments. Factors affecting N3-4 biosorption, including the amount of N3-4, temperature, pH, contact time, and initial Ca^{2+} concentration, were analyzed separately. N3-4 was added into beef paste peptone liquid medium at a 5% ratio and incubated with shaking at 30°C and 140 rpm for 48 h. The cells were then centrifuged at $8000 \times g$ for 10 min. The obtained cell precipitates were washed twice with sterilized ultrapure water, collected, and stored at 4°C for further use.

Different amounts of N3-4 cell precipitates were added to 50 ml $CaCl_2$ solution (100 mg/l Ca^{2+}, pH 6.7 ± 0.1) for incubation, and the final cell concentrations were 0.5, 1.0, 1.5, 2.0, 2.5, and 3.0 g/l (wet weight), respectively. The samples were shaken at 30°C for 60 min at 140 rpm and then centrifuged at $8000 \times g$ for 10 min. The Ca^{2+} concentration in the supernatant was measured using an atomic absorption spectrophotometer (AA 6880; Shimadzu, Japan).

To test temperature, the final cell concentration of N3-4 cell sedimentation was 2.0 g/l (wet weight) and the samples were incubated at 20, 25, 30, 35, and 40°C. All the other conditions were identical to those described above. Similarly, the pH (4, 5, 6, 7, 8, and 9),

contact time (20, 40, 60, 80, 100, and 120 min), and initial Ca^{2+} concentration (50, 100, 150, 200, 250, and 300 mg/l) were determined separately.

The biosorption capacity of N3-4 was calculated as follows (Long et al. 2019):

$$q = \frac{(C_0 - C_e) \times V}{M} \quad (1)$$

where q is the biosorption capacity (μg/g), C_0 is the initial Ca^{2+}concentration (mg/l), C_e is the final Ca^{2+} concentration in equilibrium (mg/l), V is the $CaCl_2$ solution volume (l), and M is the bacterial mass of N3-4 (g).

Ca^{2+} biosorption optimization via RSM. The Ca^{2+} biosorption conditions using strain N3-4 were further optimized using the Box-Behnken design, which uses three factors and three levels.

Single-factor experiments were conducted based on Choińska-Pulit et al. (2018) with slight modifications. The key factors selected affecting the biosorption capacity of N3-4 included the initial Ca^{2+} concentration (A: 50, 100, 150 mg/l), contact time (B: 40, 60, 80 min), and N3-4 dosage level (C: 1, 1.5, 2 g/l).

Design-Expert v12 (Stat-Ease Inc., USA) was used to statistically analyze the experimental data, which were fitted using a linear regression model (Eq. 2) (Mathew and Krishnamurthy 2018):

$$Y = \beta_0 + \Sigma_{i=1}^{3} \beta_i X_i + \Sigma_{i=1}^{3} \beta_{ii} X_i^2 \Sigma_{i=1}^{3} \Sigma_{j=i+1}^{3} \beta_{ij} X_i X_j \quad (2)$$

where Y represents the predicted response (biosorption capacity), β_0 is the model constant, while, β_i, β_{ii} and β_{ij} represent the linear, quadratic, and interaction coefficients, respectively. X_1, X_2, and X_3 correspond to the independent variables (calcium ions, contact time, and N3-4 dosage level).

This model evaluates the effects of each variable and their interactions on the responses. Fisher's test (F = 95% confidence level) and p-values ($p < 0.05$) were used to evaluate the significance of each term. Finally, the RSM was used to visualize the interactions between the operating parameters in 3D graphs and contour plots. Analysis of variance (ANOVA) was used to test the model's adequacy and the regression coefficients' statistical significance. Response surface contour plots were used to analyze interactions among the variables and their corresponding effects (Wang et al. 2015). Additional experiments were conducted to verify the optimal conditions.

Scanning electron microscopy and energy dispersive X-ray spectroscopy (SEM-EDS) analysis. The surface characteristics and element types of bacterial adsorbent N3-4 were investigated before and after Ca^{2+} biosorption using a scanning electron microscope (SEM, JSM-5600LV; JEOL Ltd., Japan) equipped with an X-ray energy chromatograph.

Biosorption was completed under the optimal conditions, as described above. In the control group, the $CaCl_2$ solution was replaced with sterilized ultrapure water. Cells were obtained by centrifugation at 8000 × g for 10 min and then dried at 30°C.

Before microscope observations, the dried cell powder was dispersed on double-sided conductive adhesive tape, coated with carbon using the arc discharge method, and sputtered with gold for 40 s (Muñoz et al. 2016). The samples were scanned to determine the morphology of the secondary electrons under an accelerating voltage of 20 kV.

Fourier transform infrared (FTIR) analysis. The chemical composition of N3-4 cells was analyzed before and after Ca^{2+} biosorption using a Nexus 670 FTIR spectrometer, which has a spectral resolution of 4 cm^{-1}. The dried cell samples were embedded in KBr pellets for detection. In total, 32 spectral scans were recorded in the transmittance band mode between 500–4,000 cm^{-1} to achieve an acceptable signal-to-noise ratio (Banerjee et al. 2019).

Statistical analysis. ANOVA and Duncan's test were conducted to analyze statistical significance using IBM® SPSS® Statistics for Windows (IBM Corp., USA). Curves were plotted using Origin v2021 (OriginLab Corporation, USA). Design-Expert v12 (Stat-Ease Inc., USA) software was used to complete multiple linear regression.

Results and Discussion

Morphological, physiological, and biochemical characterization of N3-4. After the strain was cultured on beef paste peptone medium plates at 37°C for 48 h, the N3-4 colonies were round with smooth surfaces, neat edges, greyish-white, opaque, and metallic luster. Light microscopy showed that N3-4 was Gram-positive and flagellated.

As shown in Table I, strain N3-4 can utilize gelatine, glucose, fructose, xylose, and rhamnose, but not starch or raffinose.

Molecular identification and classification of N3-4. Traditional methods only identify microorganisms at the morphological level and, therefore, have certain limitations and uncertainties. With molecular biology's rapid advancement and PCR technology's maturation, many researchers have applied molecular identification (Sedlakova-Kadukova et al. 2019). Comparison of the 16S rRNA sequence of this strain with the NCBI database and using a phylogenetic tree showed that N3-4 had the highest homology and the closest affinity with Virgibacillus pantothenticus (Fig. 1). N3-4 was therefore identified as *V. pantothenticus*, a soil bacterium formerly known as *Bacillus pantothenticus*. This

Table I
Physiological and biochemical tests and sugar fermentation tests results of strain N3–4.

Physiological and biochemical characterization experiments		Sugar fermentation test	
Indole test	+	Glucose	+
Citrate salt test	–	Fructose	+
Methyl Red test	+	Xylose	+
V-P test	+	Rhamnose	+
Gelatin hydrolysis test	+	Sucrose	+
Starch hydrolysis test	–	Arabinose	+
/	/	Marshmallow	–
/	/	Mannitol	+

+ – positive; – – negative

is a Gram-positive, spore-forming, aerobic, mesophilic, and halotolerant bacterium (Kuhlmann et al. 2011).

Effects of different parameters on N3-4 Ca^{2+} biosorption capacity. ***Contact time.*** The effect of contact time on adsorption efficacy was examined over a time range of 20–120 min. Contact time is a pivotal factor during mass transfer processes, such as biosorption (Rouibah et al. 2023). As shown in Fig. 2a, the Ca^{2+} adsorption capacity of N3-4 increased with time until 60 min; beyond this, the capacity plateaued, indicating the limited impact of extending contact time. This plateau results from the saturation of available surface sites as Ca^{2+} penetrates further into the biosorbent and reduces biosorbent activity due to solute molecule repulsion from the bulk phase (Nasrullah et al. 2015). Hence, in subsequent studies, 60 min was preliminarily used as the optimal contact time for Ca^{2+} removal.

Initial calcium concentration. Initial concentration is pivotal for addressing the metal mass-transfer resistance between aquatic and solid phases (Long et al. 2019). As illustrated in Fig. 2b, biosorption capacity increased with initial concentration, peaking at 148.20 μg/g with a calcium content of up to 100 mg/l. Elevated initial concentrations drive metal ions to

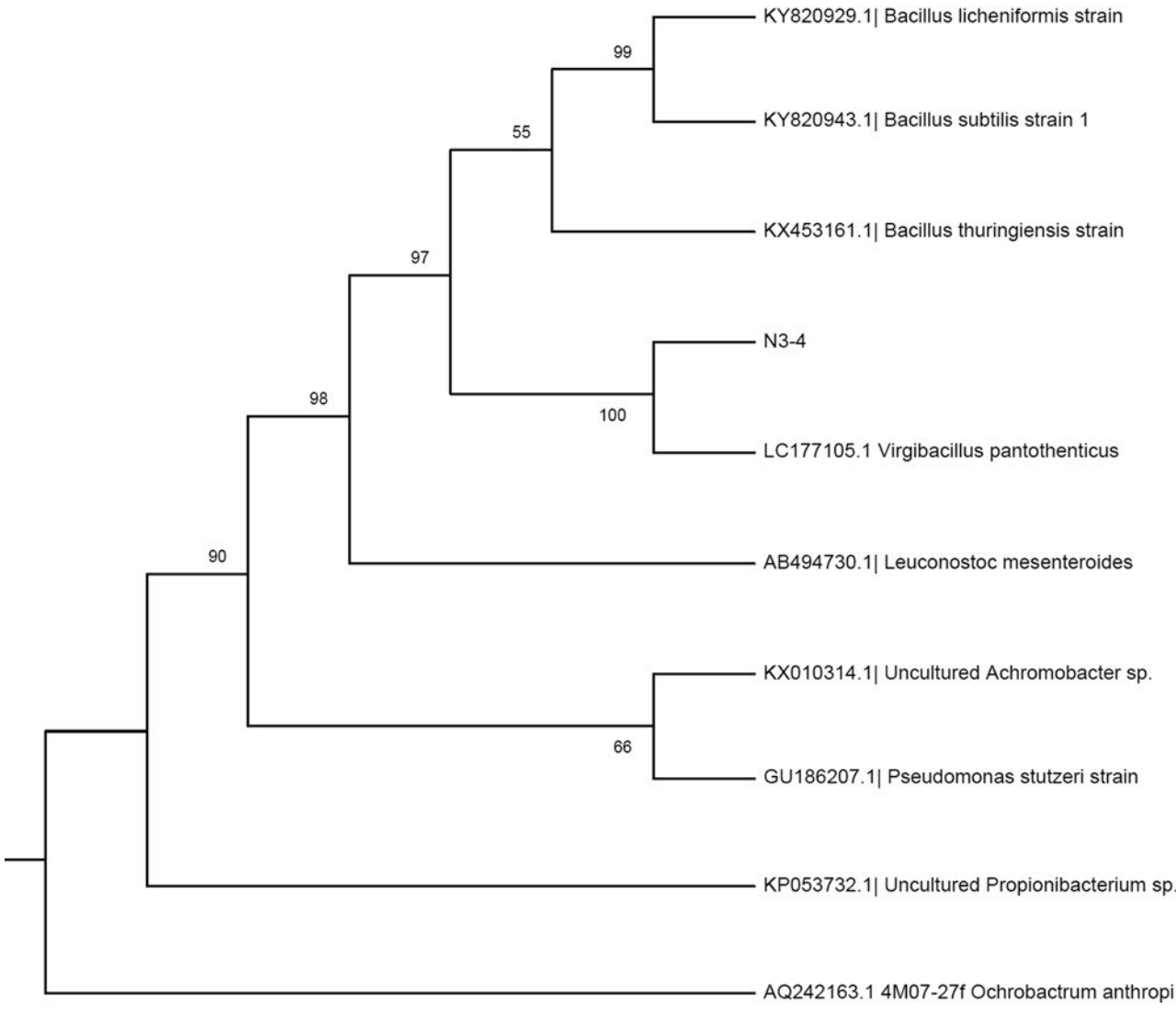

Fig 1. Phylogenetic tree of strain N3-4 based on 16S rRNA sequence.

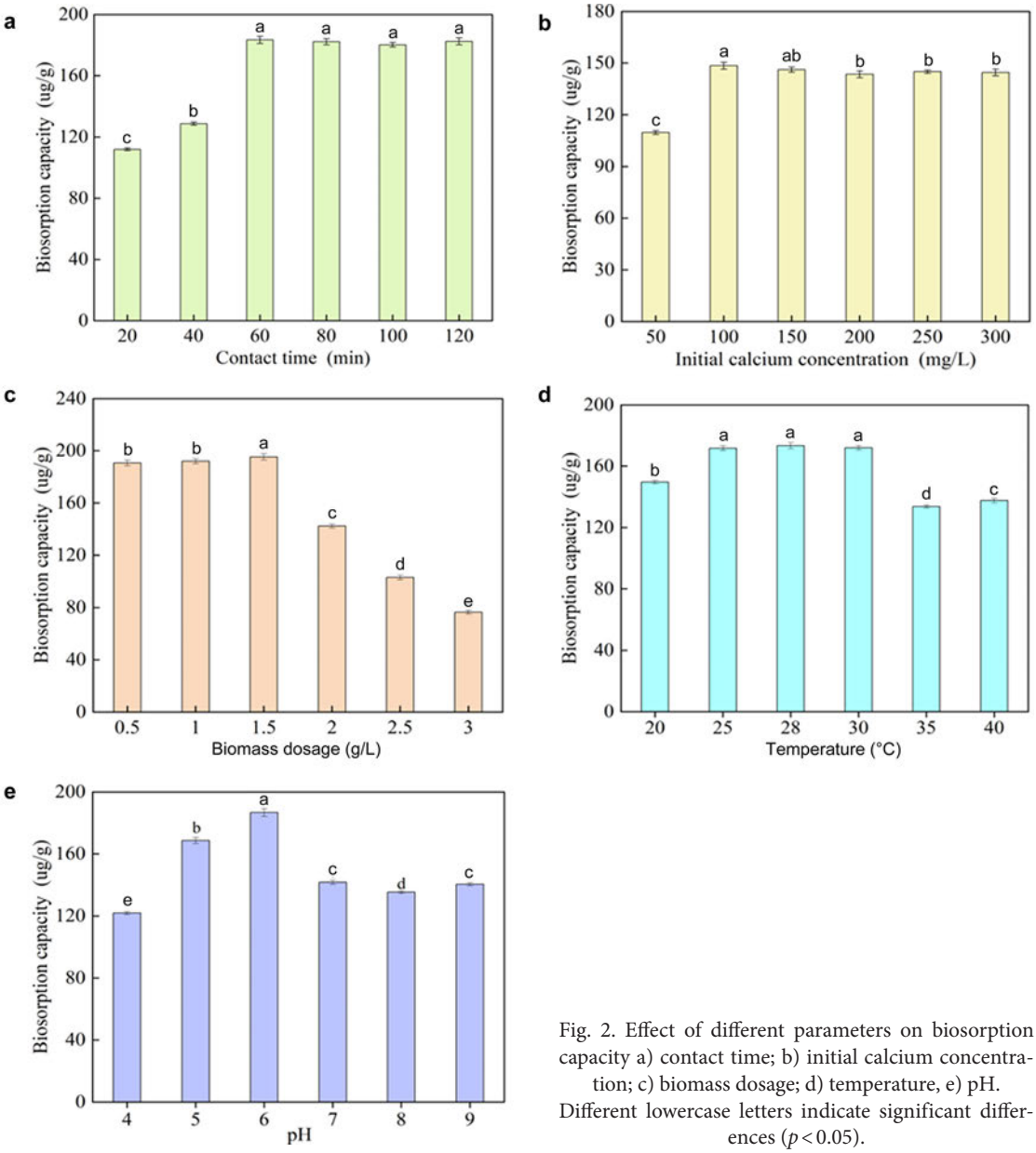

Fig. 2. Effect of different parameters on biosorption capacity a) contact time; b) initial calcium concentration; c) biomass dosage; d) temperature, e) pH. Different lowercase letters indicate significant differences ($p < 0.05$).

engage with binding sites, enhancing their adsorption (Kazy et al. 2009). However, the adsorption capacity of the biosorbent approaches saturation with increasing initial calcium concentration, given the finite availability of binding sites (Xu et al. 2015).

Biomass dosage. Assessing the dose effect is crucial for gauging biosorption capabilities (Tangestani et al. 2021). The correlation between biomass dosage and Ca^{2+} adsorption is shown in Fig. 2c. Adsorption capacity increased with increasing biomass dosage up to 1.5 g/l, peaking at 195.33 µg/g. Beyond 1.5 g/l, adsorption efficacy decreased. The reduction in adsorption capacity with higher biosorbent dosage is primarily due to increased unsaturated adsorption sites during the biosorption process. Another plausible factor is particle interaction and aggregation, which can reduce the total active surface area of the biosorbent (Long et al. 2019).

Temperature. As shown in Fig. 2d, as the temperature increased from 20 to 30°C, the biosorption capacity of N3-4 continued to increase from 149 to 173 µg/g. However, a precipitous drop was observed at 35°C, followed by a subtle increment post-35°C. Elevated temperatures induce alterations in the microbial cell surface architecture, functional group distribution, and membrane fluidity, leading to diminished adsorptive capacity (Yang et al. 2017).

pH. pH significantly impacts biosorption efficacy, given the presence of key binding sites on the adsorbent surface and metal ion hydrolysis (Afraz et al. 2020). pH alterations affect the surface charge of cells, the protonation or deprotonation states of functional groups, and membrane permeability (Yuan et al. 2019). Ca^{2+} adsorption by the bacteria was evaluated across a pH range of 4–9. As illustrated in Fig. 2e, pH significantly

Table II
Experimental and predicted response for calcium biosorption using *Virgibacillus pantothenticus*.

Run order	A Initial calcium concentration	B Contact time	C Biomass dosage	Biosorption capacity
1	150	60	1.0	540.47
2	100	60	1.5	506.53
3	100	60	1.5	507.36
4	50	60	1.0	407.77
5	100	60	1.5	517.87
6	50	40	1.5	300.87
7	50	80	1.5	432.80
8	50	60	2.0	301.13
9	150	60	2.0	451.23
10	150	40	1.5	452.42
11	100	80	1.0	520.87
12	100	60	1.5	514.87
13	100	40	2.0	314.55
14	150	80	1.5	559.02
15	100	60	1.5	529.02
16	100	80	2.0	439.98
17	100	40	1.0	417.93

affected calcium ion uptake. Adsorption capacity was positively correlated with pH values < 6, with an apex of 186.76 μg/g observed at pH 6. Adsorption efficacy declined sharply at pH values >6 and moderately increased beyond 7.

Ca^{2+} biosorption parameter optimization by RSM. RSM is a compilation of statistical and mathematical techniques built on fitting polynomial equations to experimental data (Luong et al. 2023). When multiple factors are involved, their interactions cannot be measured with single-factor experiments, even if they are dominant and many experiments are needed. However, using a reduced number of runs, RSM can evaluate independent variables and their interactions with dependent variables (Bhateria and Dhaka 2019). Multiple factors influence biosorption efficiency; therefore, RSM was employed.

In previous experiments, the initial concentration of calcium ions, biomass dosage, and contact time of bacteria significantly affected calcium ion biosorption. These adsorption experiments were carried out at room temperature and in alkaline wastewater. The one-way experiments clearly show that a temperature of 25–30°C has little effect on adsorption, and the maximum metal ion adsorbed was at pH 6. Therefore, the adsorption of metal ions with this strain was carried out at pH 6 and 28°C using the Box-Behnken model. The initial calcium concentration, contact time, and biomass dosage were selected for a three-factor, three-level response surface test using biosorption capacity as an indicator. Seventeen experiments were performed for three independent process parameters, and their interactions were studied. The experimental designs, as well as observed and predicted values are presented in Table II.

The interactions between the variables and response were evaluated using a second-order polynomial equation. The observed relationship between the biosorption capacity and input test variables in coded terms can be expressed as follows:

$$\text{Biosorption capacity } (\mu g/g) = 515.13 + 70.16A + 58.45B - 47.52C - 6.16AB + 4.35AC + 5.62BC - 38.43A^2 - 40.25B^2 - 51.55C^2 \quad (3)$$

where A, B, and C are independent singular factors, AB, AC, and BC are interaction factors, and A^2, B^2, and C^2 are the quadratic terms. The theoretical optimum value calculated from Eq. 3 was 572.43 μg/g and the actual optimum adsorption rate under optimum conditions was 561.95 μg/g.

A good model for calcium biosorption was established via ANOVA using *V. pantothenticus* biomass as an adsorbent. Statistical testing of the regression equations was performed using *F*-tests, and ANOVA for the fitted quadratic polynomial model of removal efficiency is shown in Table III. ANOVA was performed using Fisher's *F*-test. *p*-Values < 0.05 indicated that the model terms were significant. In this case, A, B, C, A^2, B^2, and C^2 were significant model terms. Values > 0.1 indicated that the model terms were not significant. An *F*-value of 236.49 implies the model was significant ($p < 0.01$). There was only a 0.01% chance that this large *F*-value could have been caused by noise. R^2 was used to determine the quality of the proposed model (Ni'mah et al. 2022). When the correlation coefficient approached 1, the prediction precision of the model improved. The R^2 and adjusted R^2 were close to 1 (0.9968 and 0.9928, respectively), indicating a strong correlation between the observed and predicted values (Garg et al. 2014). The R^2 and adjusted R^2 values indicate that the structure of the model reflects the variation in the calcium biosorption capacity relative to changes in the initial calcium concentration, biomass dosage, and contact time.

A lack-of-fit was applied to measure the adequacy of the model. A lack-of-fit test will not be significant if the model matches the data well (Shabanizadeh and Taghavijeloudar 2023). An *F*-value of 0.14 implies that the lack-of-fit was not significant relative to pure error; there was a 93.40% chance that the lack-of-fit *F*-value occurred due to noise. The accuracy of the model (Adeq) measures the model noise (ratio of information to error) (Ding et al. 2023). A ratio > 4 is desirable. The adequate precision ratio was 46.205, which indicated an adequate signal. This model can be used to navigate design space.

Response surface analysis. Under pH 6 and a temperature of 28°C, the optimal calcium adsorp-

Table III
ANOVA results for calcium biosorption parameters.

Source	Sum of squares	df	Mean square	*F* value	*p*-value	Significance
Model	1.121E+005	9	12459.59	236.49	< 0.0001	***
A	39379.40	1	39379.40	747.46	< 0.0001	***
B	27332.39	1	27332.39	518.79	< 0.0001	***
C	18064.25	1	18064.25	342.88	< 0.0001	***
AB	151.54	1	151.54	2.88	0.1337/	
AC	75.69	1	75.69	1.44	0.2697/	
BC	126.45	1	126.45	2.40	0.1653/	
A^2	6217.97	1	6217.97	118.02	< 0.0001	***
B^2	6820.04	1	6820.04	129.45	< 0.0001	***
C^2	11189.61	1	11189.61	212.39	< 0.0001	***
Residual	368.79	7	52.68	/	/ /	
Lack of Fit	33.95	3	11.32	0.14	0.9340/	
Pure Error	334.84	4	83.71	/	/	/
Cor Total	1.125E+005	16	/	/	/	/
R^2	0.9968/	/	/	/	/	
Adj: R^2	0.9928/	/	/	/	/	

*** – the difference is very significant ($p < 0.001$); ** – the difference height is significant ($p < 0.01$);
* – the difference was significant ($p < 0.05$)

tion parameters for strain N3-4 were determined to be a contact time of 72.70 minutes, an initial Ca2+ concentration of 141.98 mg/l, and a biomass dosage of 1.30 g/l. The theoretical maximum calcium adsorption was found to be 572.43 μg/g. Five parallel experiments were conducted under the same conditions to validate these findings, resulting in an error margin of only 1.83% compared to the theoretical value.

3D surface plots are graphical diagrams of regression equations showing two factors; all other factors were maintained at fixed levels (Hadiani et al. 2018). The impacts of the interactions between factors were examined using 3D surface plots (Kamani et al. 2018), which represented both the main and interaction effects of the variables well.

The response value of the response surface plot is composed of two interactions of each test factor, A, B, and C, as well as the interaction between the optimal parameters and each other parameter; the more complex and steep the surface, the more significant the influence of each factor on the response value. Each point on the same contour represents the same value, and the contour shape reflects the significance of the interaction between the factors. In the case of an elliptical contour, the corresponding contour line will also exhibit an elliptical shape, indicating that the interactions among the factors are significantly different. Conversely, if the contour is circular, this suggests that the differences in interactions among the factors are not significant.

Initial calcium concentration and contact time. The combined effects of the adsorbent and initial calcium ion concentrations are illustrated in Fig. 3a and b, with the median biomass dosage. The lowest observed biosorption capacity was 300.87 μg/g with an initial calcium concentration of 50 mg/l and a contact time of 40 min. This capacity reached a high of 559.73 μg/g at an initial calcium concentration of 150 mg/l and a contact time of 80 min. Adsorption capacity increased with initial calcium ion concentration at a fixed contact time. Conversely, at a constant initial calcium ion concentration, adsorption capacity increased with increasing contact time. Consequently, both initial calcium ion concentration and contact duration enhanced Ca^{2+} biosorption efficacy (Ding et al. 2023). Ca^{2+} ion adsorption capacity consistently increased with increased initial calcium concentration and contact time until equilibrium was reached.

This echoes Samuel et al. (2015), who presented analogous 3D response plots based on the interplay between initial concentration and contact duration. Absorption spiked within the first 40 min and reached equilibrium at approximately 60 min, with a noticeable increase in biosorption capacity with elongated contact periods.

Effect of initial calcium concentration and biomass dosage. A holistic view of the impact of the adsorbent and initial calcium ion concentration can be drawn from Fig. 3c and 3d, while median contact time was maintained. Ca^{2+} extraction rate increased with increasing initial calcium ion concentrations. Peak Ca^{2+} removal (540.47 μg/g) was observed at a biomass dosage of 2.5 g/l and an initial calcium ion concentration of approximately 100 mg/l. For a specific biomass dosage,

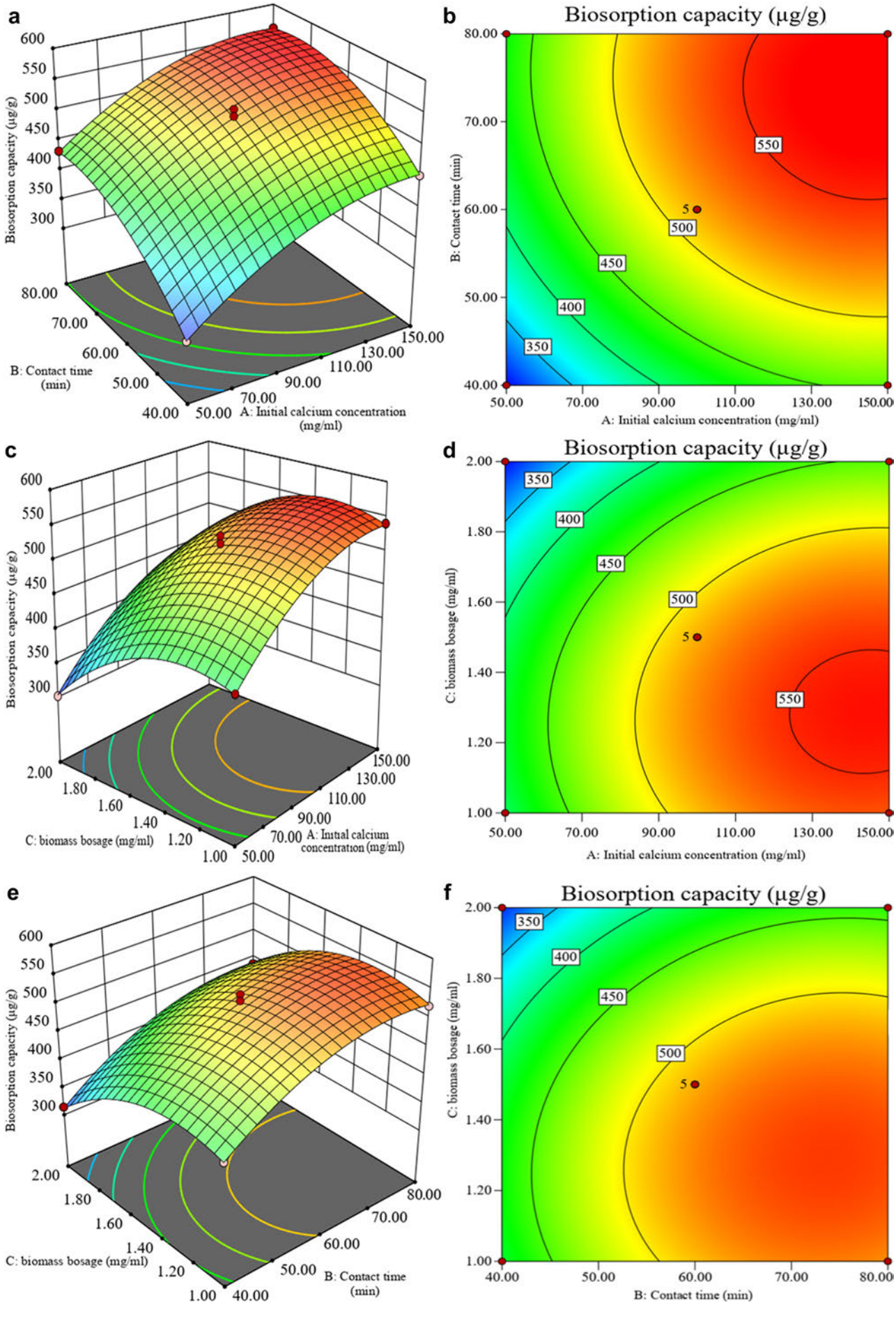
a
Biosorption capacity (µg/g)
600
550
500
450
400
350
300
80.00
70.00
60.00
50.00
40.00
B: Contact time (min)
50.00
70.00
90.00
110.00
130.00
150.00
A: Initial calcium concentration (mg/ml)
b
Biosorption capacity (µg/g)
80.00
70.00
60.00
50.00
40.00
B: Contact time (min)
550
500
450
400
350
5
50.00
70.00
90.00
110.00
130.00
150.00
A: Initial calcium concentration (mg/ml)
c
Biosorption capacity (µg/g)
600
550
500
450
400
350
300
2.00
1.80
1.60
1.40
1.20
1.00
C: biomass bosage (mg/ml)
50.00
70.00
90.00
110.00
130.00
150.00
A: Initial calcium concentration (mg/ml)
d
Biosorption capacity (µg/g)
2.00
1.80
1.60
1.40
1.20
1.00
C: biomass bosage (mg/ml)
350
400
450
500
550
5
50.00
70.00
90.00
110.00
130.00
150.00
A: Initial calcium concentration (mg/ml)
e
Biosorption capacity (µg/g)
600
550
500
450
400
350
300
2.00
1.80
1.60
1.40
1.20
1.00
C: biomass bosage (mg/ml)
40.00
50.00
60.00
70.00
80.00
B: Contact time (min)
f
Biosorption capacity (µg/g)
2.00
1.80
1.60
1.40
1.20
1.00
C: biomass bosage (mg/ml)
350
400
450
500
5
40.00
50.00
60.00
70.00
80.00
B: Contact time (min)

Fig. 3. The binary interactions of factors of calcium biosorption capacity by response surface and contour a) and b) contact time and initial calcium ion concentration interact to affect the contour of bacterial adsorption capacity; c) and d) Biomass dosage and initial calcium ion concentration affects contours of bacterial adsorption capacity; e) and f) Biomass dosage and contact time affects contours of bacterial adsorption capacity.

adsorption capacity spiked dramatically with increasing initial calcium ion concentrations, which is a key determinant of Ca^{2+} removal. The biosorption capacity increases at low initial biomass dosages as the initial Ca^{2+} concentration rises. The specific sites crucial for low-concentration biosorption become saturated when Ca^{2+} concentrations are elevated. Consequently, at high Ca^{2+} concentrations, further ion uptake did not occur with increased calcium ion concentrations because of saturation (Bhateria and Dhaka 2019).

Biomass dosage and contact time. Fig. 3e and 3f illustrates the interplay between biomass dosage and contact time concerning calcium biosorption capacity while maintaining median initial calcium concentration. The lowest recorded biosorption capacity was 314.55 µg/g with a biomass dosage of 2 g/l and a contact time of 40 min. This capacity surged to 520.87 µg/g when the biomass dosage was reduced to 1 g/l and contact time extended to 80 min. The gradient and curvature of the contact time surface are more pronounced than those associated with biomass dosage, indicating that the duration of the contact is the primary factor influencing adsorption capacity (Jiang et al. 2022). Each adsorbent has a finite number of adsorption sites (Soleimani et al. 2023). In addition, particle aggregation and the unsaturation of binding sites lead to a decrease in the overall accessible surface area of the adsorbent (Shukla and Pai 2005). This diminishes uptake capacity at increased biosorbent concentrations.

SEM-EDS analysis of *V. pantothenticus*. Using SEM to characterize biosorbents efficiently provides data on their morphology and elemental composition (Gupta et al. 2019). SEM-EDS provides valuable information regarding a sample's physical structure and elemental makeup.. This technique enables the detection of trace elements within micron-scale specimens with a precision that can reach submicron levels (Singh et al. 2023). SEM was therefore employed to examine surface alterations during adsorption.

Bacteria can adsorb Ca^{2+} ions through nucleation on the cell wall and within extracellular polymers, facilitating Ca^{2+} clearance (Li et al. 2022). Fig. 4 shows

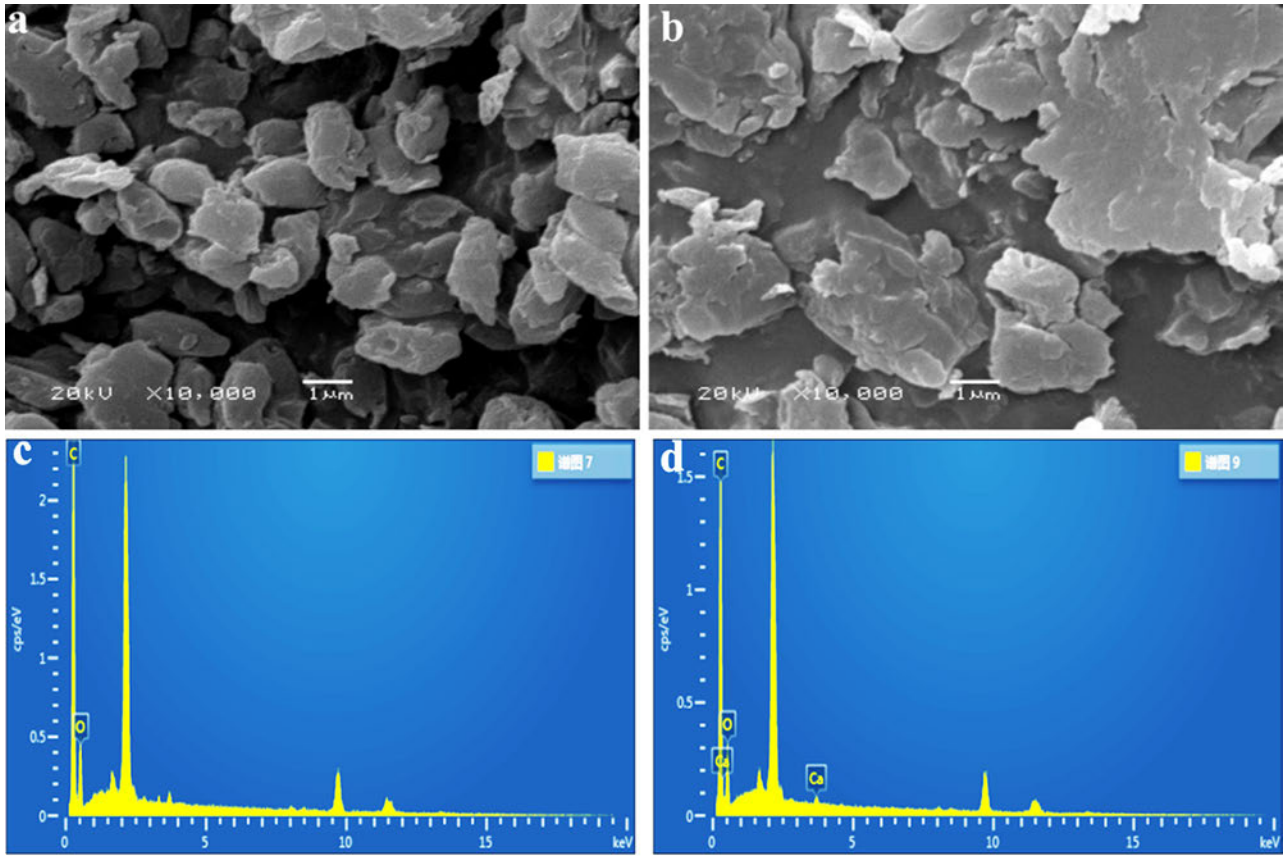

Fig. 4. SEM images and EDS spectra of *Virgibacillus pantothenticus* biomass: a) non-adsorbed biomass, b) Ca(II)-adsorbed biomass, c) EDS spectrum of non-adsorbed biomass and d) EDS spectrum of Ca(II)-adsorbed biomass.

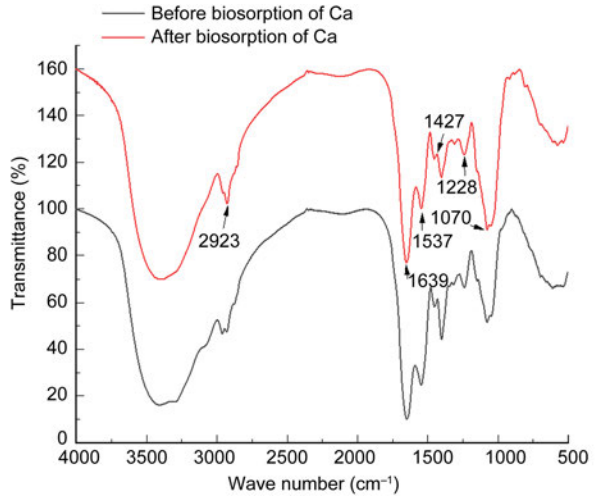

Fig. 5. FTIR spectra of *Virgibacillus pantothenticus* cells before and after calcium biosorption.

SEM-EDS analysis of the interaction mechanisms of Ca^{2+} elimination by *V. pantothenticus*. Electron micrographs of untreated bacterial cells are shown in Fig. 4a, revealing a smooth terrain (Das et al. 2014), which indicates a consistent distribution of elements across bacterial cell surfaces. This indicates a uniform distribution of components on the bacterial cell surface. Ca^{2+}-treated bacteria formed clusters and large particles with dense structures on the surface. This suggests that the aggregation of metal ions was facilitated by their attachment to the hydrophilic groups of peptides, leading to the formation of densely packed particles (Qi et al. 2023). As shown in Fig. 4b, the surface of Ca^{2+}-treated bacterial cells was rough, with bulges and sediments, which may have been caused by extracellular polymers that contribute to heavy metal binding (Yang et al. 2017). Extracellular polymeric substances reacting with calcium form sediments. The appearance of irregular bulges in the cells may have been caused by the exchange of mechanical forces and metal ions with active functional groups on the cell surface (Kazy et al. 2009; Sharma et al. 2022).

Distinct calcium peaks were discernible in the calcium-enriched biomass but absent in its untreated counterpart, confirming the presence of calcium on the surface, as shown in Fig. 4d. Notably, pronounced carbon and oxygen peaks were observed in the EDS spectra of both Ca^{2+}-adsorbed and -unadsorbed biomass, suggesting their inherent presence in the biomass and their potential involvement in metal biosorption ion exchange dynamics (Dixit et al. 2015).

FTIR analysis of *V. pantothenticus*. FTIR spectroscopy is a powerful technique that determines the vibrational properties of molecular compounds. By probing molecular vibrations, FTIR determines the presence of- and changes in functional groups and improves our understanding of surface interactions, especially during processes such as biosorption (Gupta et al. 2019; Mekpan et al. 2025). Shifts in FTIR absorption peaks are a reliable indicator of chemical structure modifications and indicate the interactions between metal ions and organic ligands at the molecular level (Qi et al. 2023). Each molecule exhibits a specific vibrational signature due to its unique bond vibrations. Distinctive FTIR spectra emerge for these unique molecular vibrations (Deng et al. 2022).

The FTIR spectra of free and calcium-loaded cells were analyzed to identify the functional groups responsible for Ca^{2+} binding. As shown in Fig. 5, the cell surface exhibited multiple characteristic peaks before adsorption, suggesting the intricate nature of the strain (Li et al. 2018). In the calcium-loaded bacterial spectrum, the broad and intense band at 3,200–3,600 cm^{-1} represents the –OH (Nagarajan et al. 2023) and/ $-NH_2$ symmetric stretching vibrations from hydroxyl or amino groups (Long et al. 2019). Meanwhile, the peaks at 2,923 cm^{-1} and 1,639 cm^{-1} signify aliphatic stretching and C≡C stretching in aromatic rings (Wang et al. 2014); these shifted approximately 10 cm^{-1} and 5 cm^{-1}, respectively, compared to the control biomass. The peak at 1,537 cm^{-1} was ascribed to the amide (II) stretching of aromatic rings (Isik et al. 2021) is crucial for bacterial identification using FTIR spectroscopy.

The FTIR spectrum of calcium-loaded *V. pantothenticus* featured a characteristic amide bond at 1,537 cm^{-1}. The 1,434 cm^{-1} peak can be linked to the C–O bond of the carboxyl group, accompanied by S = O stretching (Nagy et al. 2014). Another significant adsorption peak at 1,427 cm^{-1} corresponds to C = O stretching vibrations of amide I and $-CH_2$ bending (Banerjee et al. 2019), which shifted approximately 5 cm^{-1} from the control biomass. The unique peaks for Ca-loaded V. pantothenticus at 1,228 cm^{-1} and 1,070 cm^{-1} suggest that the stretching of C = O and –C–N in amino groups plays a role in Ca^{2+} binding (Chakravarty and Banerjee 2012). These peaks also shifted approximately 10 cm^{-1} and 15 cm^{-1}, respectively, compared with the control cells. Lastly, the –C–O– or –C–N group-associated biosorption peak transitioned from 1,051 cm^{-1} to 1,074 cm^{-1}, denoting the potential interaction between these groups and metal ions (Choińska-Pulit et al. 2018).

Ca^{2+} removal mechanism. Bacteria are formidable natural scavengers that eff convert heavy metals into less harmful forms or stabilize them in solid structures (Chaudhary et al. 2021; Sharma and Shukla 2021; Sharma et al. 2022). Microbial communities found near industrial dumps and waste sites demonstrate a natural resilience to heavy metals. The existing literature indicates that these microorganisms have undergone evolutionary adaptations that enable them to effectively absorb heavy metals (Mejias Carpio et al. 2018). *Klebsiella* sp. AW2 was isolated from the rhizosphere of

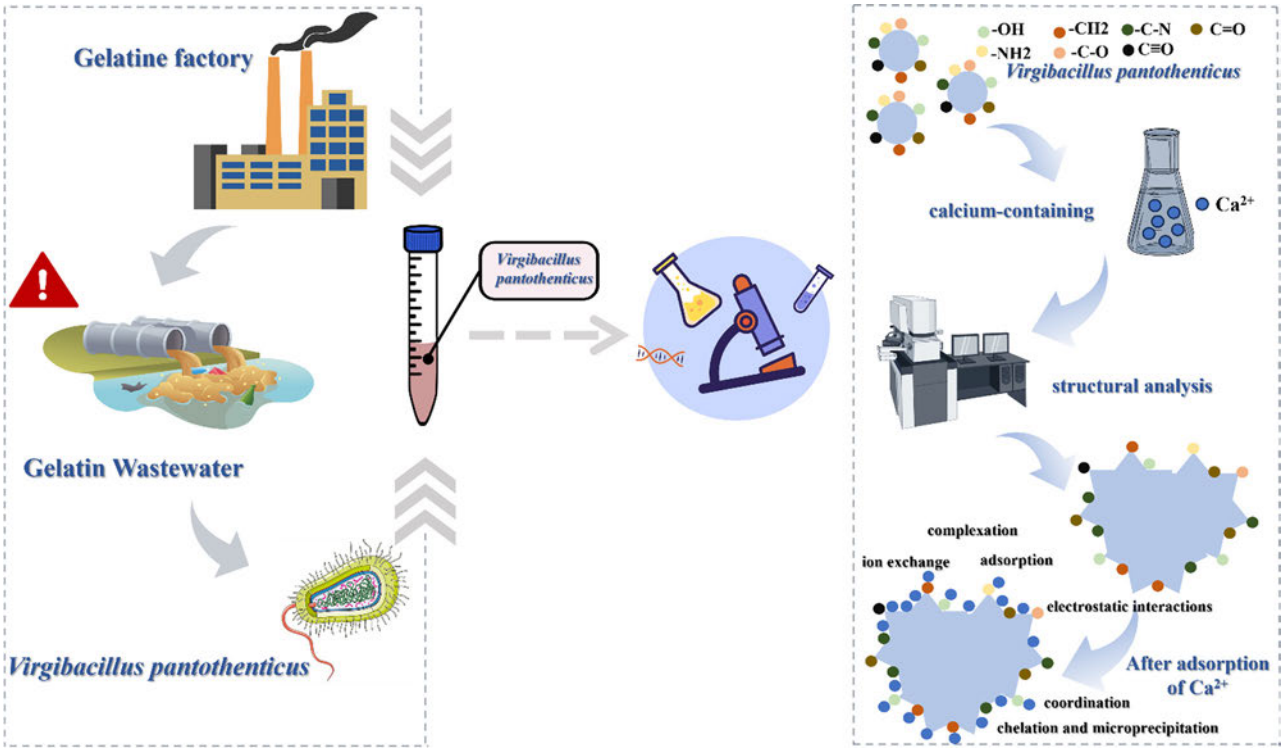

Fig. 6. Schematic diagram of the adsorption mechanism of *Virgibacillus pantothenticus*.

Solanum nigrum and exhibited tolerance to 240 mg/l of Cd^{2+} (Chi et al. 2024). The study focused on removing chromium (Cr) from water using biosorbents from live and dead *Bacillus nitratireducens* cells, isolated from textile wastewater, which tolerated Cr concentrations up to 1,000 mg/l MIC (Imron et al. 2024). The study enriched rare earth elements from aqueous solutions using *Bacillus* spp. strain DW015 and the urease-producing strain *Sporosarcina pasteurii* are isolated from ion-adsorbed rare earth ores (Bian et al. 2024).

The cell wall is the initial cellular structure that encounters metal ions. Metal biosorption by non-living biomaterials occurs through the complexation between metal ions and various functional groups, including carboxyl, phosphate, and hydroxyl groups found on the cell surface (Huang et al. 2020). Biosorption of heavy metals is a multifaceted process that encompasses various mechanisms (Wang et al. 2019; Liu et al. 2023b). The adsorption of metal ions onto cell surfaces, facilitated by stoichiometric interactions with metal functional groups, is called passive biosorption. This process may involve one or several mechanisms, including ion exchange, complexation, coordination, adsorption, electrostatic interactions, chelation, and microprecipitation (Kumar et al. 2022; Liu et al. 2023a). The FT-IR pattern reveals changes in peak broadening and contraction during the binding process with calcium, indicating interactions between functional groups and metal particles. The main functional groups that bind calcium ions include –OH, $–NH_2$, C=O, –C–O–, and –C–N. The adsorption of calcium ions from gelatin wastewater by the strains discussed in the article occurs through interactions with surface functional groups.

Conclusions

In this study, a bacterial strain with strong resistance to calcium ions was isolated from gelatine wastewater and identified as *V. pantothenticus* based on morphological characterization, physiological and biochemical identification, and molecular biology. The optimum adsorption conditions for calcium ions by *V. pantothenticus* were as follows: contact time, 72.68 min; biomass dosage, 1.3 g/l; initial calcium concentration, 142.01 mg/l; and maximum calcium adsorption, 572.43 μg/g. According to structural characterization via FTIR and SEM-EDS, the morphology of *V. pantothenticus* after bioabsorption was severely deformed, with a rough surface, protrusions, and sediments. Compared with pre-adsorption bacteria, post-adsorption bacteria had calcium, carbon, and nitrogen peaks, indicating that post-adsorption bacteria contained a certain amount of calcium. Functional groups, such as –OH, $–NH_2$, C≡C, C=O, $–CH_2$, –C–O–, and –C–N, were likely involved in Ca^{2+} adsorption.

Optimization somewhat improved the bacteria's calcium adsorption capacity; however, the amount of adsorption remained relatively small. To overcome the limitations of studying existing calcium-resistant

strains, future studies should expand the available calcium ion adsorption strains and aim to produce strains with higher calcium adsorption capacity. This study of a calcium-resistant strain remains at the laboratory stage and has not been further applied to gelatine wastewater treatment; further investigation is required for practical applications.

Availability of data and material

Most of the data are embedded in the manuscript and if any additional data is required, it will be made available on request.

Acknowledgements

This work was financially supported by the Gansu Provincial Higher Education Industry Support Project (Grant number 2023CYZC-23) and the Key Project of Natural Science Foundation of Gansu Province (Grant number 21JR7RA203).

Author contribution

Haiwei Ren: conceptualization, methodology, financial support, writing review and editing. Yumeng Xiang: methodology, software, validation, writing-original draft preparation, investigation. Aili Zhang: experiment and analysis, data curation. Hongyuan Zhao: methodology, writing review and editing. Hui Tian: Experiment and analysis, writing review and editing. Xiaopeng Guo: writing review and editing, supervision. Yi Zheng: writing review and editing. Bingyun Zhang: methodology.

Conflict of interest

The authors do not report any financial or personal connections with other persons or organizations, which might negatively affect the contents of this publication and/or claim authorship rights to this publication.

Literature

Afraz V, Younesi H, Bolandi M, Hadiani MR. Optimization of lead and cadmium biosorption by *Lactobacillus acidophilus* using response surface methodology. Biocatal Agric Biotechnol. 2020 Oct; 29:101828. https://doi.org/10.1016/j.bcab.2020.101828

Awasthi MK, Pandey AK, Bundela PS, Wong JWC, Li R, Zhang Z. Co-composting of gelatin industry sludge combined with organic fraction of municipal solid waste and poultry waste employing zeolite mixed with enriched nitrifying bacterial consortium. Bioresour Technol. 2016 Aug;213:181–189. https://doi.org/10.1016/j.biortech.2016.02.026

Banerjee S, Kamila B, Barman S, Joshi SR, Mandal T, Halder G. Interlining Cr(VI) remediation mechanism by a novel bacterium *Pseudomonas brenneri* isolated from coalmine wastewater. J Environ Manage. 2019 Mar;233:271–282. https://doi.org/10.1016/j.jenvman.2018.12.048

Bhateria R, Dhaka R. Optimization and statistical modelling of cadmium biosorption process in aqueous medium by *Aspergillus niger* using response surface methodology and principal component analysis. Ecol Eng. 2019 Sep;135:127–138. https://doi.org/10.1016/j.ecoleng.2019.05.010

Bian Z, Dong W, Li X, Song Y, Huang H, Hong K, Hu K. Enrichment of Terbium(III) under synergistic effect of biosorption and biomineralization by *Bacillus* sp. DW015 and *Sporosarcina pasteurii*. Microbiol Spectr. 2024 Aug;12(8):e0076024. https://doi.org/10.1128/spectrum.00760-24

Chakravarty R, Banerjee PC. Mechanism of cadmium binding on the cell wall of an acidophilic bacterium. Bioresour Technol. 2012 Mar;108:176–183. https://doi.org/10.1016/j.biortech.2011.12.100

Chaudhary P, Beniwal V, Umar A, Kumar R, Sharma P, Kumar A, Al-Hadeethi Y, Chhokar V. *In vitro* microcosm of co-cultured bacteria for the removal of hexavalent Cr and tannic acid: A mechanistic approach to study the impact of operational parameters. Ecotoxicol Environ Saf. 2021 Jan;208:111484. https://doi.org/10.1016/j.ecoenv.2020.111484

Chi Y, Wang R, Zhang X, Ma X, Qin T, Zhang D, Chu S, Zhao T, Zhou P, Zhang D. Identification of cadmium-tolerant plant growth-promoting rhizobacteria and characterization of its Cd-biosorption and strengthening effect on phytoremediation: Development of a new amphibious-biocleaner for Cd-contaminated site. J Environ Manage. 2024 Dec;371:123225. https://doi.org/10.1016/j.jenvman.2024.123225

Choińska-Pulit A, Sobolczyk-Bednarek J, Łaba W. Optimization of copper, lead and cadmium biosorption onto newly isolated bacterium using a Box-Behnken design. Ecotoxicol Environ Saf. 2018 Mar;149:275–283. https://doi.org/10.1016/j.ecoenv.2017.12.008

Das S, Mishra J, Das SK, Pandey S, Rao DS, Chakraborty A, Sudarshan M, Das N, Thatoi H. Investigation on mechanism of Cr(VI) reduction and removal by *Bacillus amyloliquefaciens*, a novel chromate tolerant bacterium isolated from chromite mine soil. Chemosphere. 2014 Feb;96:112–121. https://doi.org/10.1016/j.chemosphere.2013.08.080

Deng G, Nagy C, Yu P. Combined molecular spectroscopic techniques (SR-FTIR, XRF, ATR-FTIR) to study physiochemical and nutrient profiles of Avena sativa grain and nutrition and structure interactive association properties. Crit Rev Food Sci Nutr. 2023; 63(25):7225–7237. https://doi.org/10.1080/10408398.2022.2045470

Ding E, Jiang J, Lan Y, Zhang L, Gao C, Jiang K, Qi X, Fan X. Optimizing Cd^{2+} adsorption performance of KOH modified biochar adopting response surface methodology. J Anal Appl Pyrolysis. 2023Jan;169:105788. https://doi.org/10.1016/j.jaap.2022.105788

Dixit R, Wasiullah, Malaviya D, Pandiyan K, Singh UB, Sahu A, Shukla R, Singh BP, Rai JP, Sharma PK, et al. Bioremediation of heavy metals from soil and aquatic environment: An overview of principles and criteria of fundamental processes. Sustainability. 2015 Feb;7(2):2189–2212. https://doi.org/10.3390/su7022189

Elsayed AE, Attia SK, Mahmoud GA, Mostafa YM, Taman AR, Osman DI. Environmentally friendly radiation EDTA modified hydrogel based on gelatin for adsorptive removal of cationic and anionic dye from synthetic wastewater. Egypt J Pet. 2023 Dec;32(4):30–35. https://doi.org/10.1016/j.ejpe.2023.10.002

Garg SK, Tripathi M, Lal N. Response surface methodology for optimization of process variable for reactive orange 4 dye discoloration by *Pseudomonas putida* SKG-1 strain and bioreactor trial for its possible use in large-scale bioremediation. Desalin Water Treat. 2014 Jun;54(11):3122–3133. https://doi.org/10.1080/19443994.2014.905975

Gupta S, Sharma SK, Kumar A. Biosorption of Ni(II) ions from aqueous solution using modified *Aloe barbadensis* Miller leaf powder. Water Sci Eng. 2019 Mar;12(1):27–36. https://doi.org/10.1016/j.wse.2019.04.003

Hadiani MR, Darani KK, Rahimifard N, Younesi H. Biosorption of low concentration levels of Lead (II) and Cadmium (II) from aqueous solution by *Saccharomyces cerevisiae*: Response surface methodology. Biocatal Agric Biotechnol. 2018 Jul;15:25–34. https://doi.org/10.1016/j.bcab.2018.05.001

Hansda A, Kumar V, Anshumali. A comparative review towards potential of microbial cells for heavy metal removal with emphasis on biosorption and bioaccumulation. World J Microbiol Biotechnol. 2016 Oct;32(10):170. https://doi.org/10.1007/s11274-016-2117-1

He M, Xu Y, Qiao Y, Zhang Z, Liang J, Peng Y, Liao J, Qiao Y, Shang C, Guo Z, et al. A novel yeast strain *Geotrichum* sp. CS-67 capable of accumulating heavy metal ions. Ecotoxicol Environ Saf. 2022 May;236:113497. https://doi.org/10.1016/j.ecoenv.2022.113497

Huang Y, Li M, Yang Y, Zeng Q, Loganathan P, Hu L, Zhong H, He Z. *Sulfobacillus thermosulfidooxidans*: An acidophile isolated from acid hot spring for the biosorption of heavy metal ions. Int. J. Environ. Sci. Technol. 2020 May;17:2655–2666. https://doi.org/10.1007/s13762-020-02669-1

Imron MF, Setiawan W, Putranto TWC, Abdullah SRS, Kurniawan SB. Biosorption of chromium by live and dead cells of *Bacillus nitratireducens* isolated from textile effluent. Chemosphere. 2024 Jul; 359:142389. https://doi.org/10.1016/j.chemosphere.2024.142389

Isik B, Ugraskan V, Cankurtaran O. Effective biosorption of methylene blue dye from aqueous solution using wild macrofungus (*Lactarius piperatus*). Sep Sci Technol. 2021 Jul;57(6):854–871. https://doi.org/10.1080/01496395.2021.1956540

Jiang C, Yue F, Li C, Zhou S, Zheng L. Polyethyleneimine-modified lobster shell biochar for the efficient removal of copper ions in aqueous solution: Response surface method optimization and adsorption mechanism. J Environ Chem Eng. 2022 Dec;10(6):108996. https://doi.org/10.1016/j.jece.2022.108996

Jiao Z, Gao C, Li J, Lu J, Wang J, Li L, Chen X. Weathered coal-immobilized microbial materials as a highly efficient adsorbent for the removal of lead. Molecules. 2024 Jan;29(3):660. https://doi.org/10.3390/molecules29030660

Kamani H, Safari GH, Asgari G, Ashrafi SD. Data on modeling of enzymatic elimination of Direct Red 81 using Response Surface Methodology. Data Brief. 2018 Mar;18:80–86. https://doi.org/10.1016/j.dib.2018.03.012

Karnwal A. Unveiling the promise of biosorption for heavy metal removal from water sources. Desalin Water Treat. 2024 Jul; 319: 100523. https://doi.org/10.1016/j.dwt.2024.100523

Kazy SK, D'Souza SF, Sar P. Uranium and thorium sequestration by a *Pseudomonas* sp.: Mechanism and chemical characterization. J Hazard Mater. 2009 Apr;163(1):65–72. https://doi.org/10.1016/j.jhazmat.2008.06.076

Kuhlmann AU, Hoffmann T, Bursy J, Jebbar M, Bremer E. Ectoine and hydroxyectoine as protectants against osmotic and cold stress: Uptake through the SigB-controlled betaine-choline- carnitine transporter-type carrier EctT from *Virgibacillus pantothenticus*. J Bacteriol. 2011 Sep;193(18):4699–4708. https://doi.org/10.1128/jb.05270-11

Kumar U, Singh RS, Mandal J, Nayak AK, Jha AK. Removal of As(III) and Cr(VI) from aqueous solutions by *Bixa orellana* leaf biosorbent and As(III) removal using bacterial isolates from heavy metal contaminated site. J Indian Chem Soc. 2022 May;99(5):100334. https://doi.org/10.1016/j.jics.2021.100334

Li D, Zhao H, Li G, Yan H, Han Z, Chi X, Meng L, Wang J, Xu Y, Tucker ME. Calcium ion biorecovery from industrial wastewater by *Bacillus amyloliquefaciens* DMS6. Chemosphere. 2022 Jul;298: 134328. https://doi.org/10.1016/j.chemosphere.2022.134328

Li X, Li D, Yan Z, Ao Y. Biosorption and bioaccumulation characteristics of cadmium by plant growth-promoting rhizobacteria. RSC Adv. 2018 Sep;8(54):30902–30911. https://doi.org/10.1039/c8ra06270f

Liu G, Geng W, Wu Y, Zhang Y, Chen H, Li M, Cao Y. Biosorption of lead ion by lactic acid bacteria and the application in wastewater. Arch Microbiol. 2023a Dec;206(1):18. https://doi.org/10.1007/s00203-023-03755-x

Liu J, Hu J, Zhong J, Luo J, Zhao A, Liu F, Hong R, Qian G, Xu ZP. The effect of calcium on the treatment of fresh leachate in an expanded granular sludge bed bioreactor. Bioresour Technol. 2011 May;102(9):5466–5472. https://doi.org/10.1016/j.biortech.2010.11.056

Liu Y, Li W, Sun X, Li S, Wang C, Zhang,R. Adsorption of lead ions by green waste compost and its mechanism. J Soils Sediments. 2023b;23(1):299–311. https://doi.org/10.1007/s11368-022-03307-8

Long J, Yuvaraja G, Zhou S, Mo J, Li H, Luo D, Chen DY, Kong L, Subbaiah MV, Reddy GM. Inactive *Fusarium* Fungal strains (ZSY and MJY) isolation and application for the removal of Pb(II) ions from aqueous environment. J Ind.Eng Chem. 2019 Apr;72:442–452. https://doi.org/10.1016/j.jiec.2018.12.047

Luong HQ, Le TN, Lee PH, Hsieh PC. Optimization of nonspecific protease activity fabrication by *Bacillus subtilis* N30 isolated from Taiwan using different models of response surface methodology. Biocatal Agric Biotechnol. 2023Jul;50:102686. https://doi.org/10.1016/j.bcab.2023.102686

Mathew BB, Krishnamurthy NB. Screening and identification of bacteria isolated from industrial area groundwater to study lead sorption: Kinetics and statistical optimization of biosorption parameters. Groundw Sustain Dev. 2018 Sep;7:313–327. https://doi.org/10.1016/j.gsd.2018.07.007

Mejias Carpio IE, Ansari A, Rodrigues DF. Relationship of biodiversity with heavy metal tolerance and sorption capacity: A meta-analysis approach. Environ Sci Technol. 2018 Jan;52(1):184–194. https://doi.org/10.1021/acs.est.7b04131

Mekpan W, Cheirsilp B, Maneechote W, Srinuanpan S. Intensification and characterization of biosorption of microalgal cells on filamentous fungal pellets as effective tools for harvesting of microalgal biomass. Sep Purif Technol. 2025 Jun;358:130316. https://doi.org/10.1016/j.seppur.2024.130316

Muñoz AJ, Espínola F, Ruiz E. Removal of Pb(II) in a packed-bed column by a *Klebsiella* sp. 3S1 biofilm supported on porous ceramic Raschig rings. J Ind Eng Chem. 2016 Aug;40:118–127. https://doi.org/10.1016/j.jiec.2016.06.012

Nagarajan K, Surumbarkuzhali N, Parimala K. Spectral analysis (FT-IR, FT-Raman, UV and NMR), molecular docking, ADMET properties and computational studies: 2-Hydroxy-5-nitrobenzaldehyde. J Indian Chem Soc. 2023 Mar;100(3):100927. https://doi.org/10.1016/j.jics.2023.100927

Nagy B, Szilagyi B, Majdik C, Katona G, Indolean C, Măicăneanu A. Cd (II) and Zn (II) biosorption on *Lactarius piperatus* macrofungus: Equilibrium isotherm and kinetic studies. Environ Prog Sustainable Energy. 2014 Dec;33(4):1158–1170. https://doi.org/10.1002/ep.11897

Nasrullah A, Khan H, Khan AS, Man Z, Muhammad N, Khan MI, Abd El-Salam NM. Potential biosorbent derived from *Calligonum polygonoides* for removal of methylene blue dye from aqueous solution. Sci World J. 2015;2015:562693. https://doi.org/10.1155/2015/562693

Ni'mah YL, Subandi APK, Suprapto S. The application of silica gel synthesized from chemical bottle waste for zinc (II) adsorption using Response Surface Methodology (RSM). Heliyon. 2022 Dec; 8(12):e11997. https://doi.org/10.1016/j.heliyon.2022.e11997

Priya AK, Gnanasekaran L, Dutta K, Rajendran S, Balakrishnan D, Soto-Moscoso M. Biosorption of heavy metals by microorganisms: Evaluation of different underlying mechanisms. Chemosphere. 2022 Nov;307(Pt_4):135957. https://doi.org/10.1016/j.chemosphere.2022.135957

Qi L, Zhang H, Guo Y, Zhang C, Xu Y. A novel calcium-binding peptide from bovine bone collagen hydrolysate and chelation mechanism and calcium absorption activity of peptide-calcium chelate. Food Chem. 2023 Jun;410:135387. https://doi.org/10.1016/j.foodchem.2023.135387

Razzak SA, Faruque MO, Alsheikh Z, Alsheikhmohamad L, Alkuroud D, Alfayez A, Hossain SMZ, Hossain MM. A comprehensive review on conventional and biological-driven heavy metals removal from industrial wastewater. Environ Adv. 2022 Apr; 7:100168. https://doi.org/10.1016/j.envadv.2022.100168

Rouibah K, Ferkous H, Delimi A, Himeur T, Benamira M, Zighed M, Darwish AS, Lemaoui T, Yadav KK, Bhutto JK, et al. Biosorption of zinc (II) from synthetic wastewater by using Inula Viscosa leaves as a low-cost biosorbent: Experimental and molecular modeling studies. J Environ Manage. 2023 Jan;326(Pt_A):116742. https://doi.org/10.1016/j.jenvman.2022.116742

Samuel MS, E A Abigail M, Ramalingam C. Biosorption of Cr(VI) *by Ceratocystis paradoxa* MSR2 using isotherm modelling, kinetic study and optimization of batch parameters using response surface methodology. PLoS One. 2015 Mar;10(3):e0118999. https://doi.org/10.1371/journal.pone.0118999

Sedlakova-Kadukova J, Kopcakova A, Gresakova L, Godany A, Pristas P. Bioaccumulation and biosorption of zinc by a novel *Streptomyces* K11 strain isolated from highly alkaline aluminium brown mud disposal site. Ecotoxicol Environ Saf. 2019 Jan;167:204–211. https://doi.org/10.1016/j.ecoenv.2018.09.123

Shabanizadeh H, Taghavijeloudar M. A sustainable approach for industrial wastewater treatment using pomegranate seeds in flocculation-coagulation process: Optimization of COD and turbidity removal by response surface methodology (RSM). J Water Process Eng. 2023 Jul;53:103651. https://doi.org/10.1016/j.jwpe.2023.103651

Sharma B, Shukla P. Lead bioaccumulation mediated by *Bacillus cereus* BPS-9 from an industrial waste contaminated site encoding heavy metal resistant genes and their transporters. J Hazard Mater. 2021 Jan;401:123285. https://doi.org/10.1016/j.jhazmat.2020.123285

Sharma R, Jasrotia T, Umar A, Sharma M, Sharma S, Kumar R, Alkhanjaf AAM, Vats R, Beniwal V, Kumar R, et al. Effective removal of Pb(II) and Ni(II) ions by *Bacillus cereus* and *Bacillus pumilus*: An experimental and mechanistic approach. Environ Res. 2022 Sep;212(Pt B):113337. https://doi.org/10.1016/j.envres.2022.113337

Shi X, Duan Z, Jing Wang, Zhou W, Jiang M, Li T, Ma H, Zhu X. Simultaneous removal of multiple heavy metals using single chamber microbial electrolysis cells with biocathode in the micro-aerobic environment. Chemosphere. 2023 Mar;318:137982. https://doi.org/10.1016/j.chemosphere.2023.137982

Shukla SR, Pai RS. Adsorption of Cu(II), Ni(II) and Zn(II) on dye loaded groundnut shells and sawdust. Sep Purif Technol. 2005 Apr;43(1):1–8. https://doi.org/10.1016/j.seppur.2004.09.003

Singh GK, Kaur R, Singh C, Singh P. Elemental analysis and characterization of vermilion and lipstick sample using SEM-EDS. Mater Today Proc. 2023. https://doi.org/10.1016/j.matpr.2022.12.180

Soleimani H, Sharafi K, Amiri Parian J, Jaafari J, Ebrahimzadeh G. Acidic modification of natural stone for Remazol Black B dye adsorption from aqueous solution- central composite design (CCD) and response surface methodology (RSM). Heliyon. 2023 Mar; 9(4):e14743. https://doi.org/10.1016/j.heliyon.2023.e14743

Tangestani M, Naeimi B, Dobaradaran S, Keshtkar M, Salehpour P, Fouladi Z, Zareipour S, Sadeghzadeh F. Biosorption of fluoride from aqueous solutions by *Rhizopus oryzae*: Isotherm and kinetic evaluation. Environ Prog Sustainable Energy. 2022 Jan;41(1):e13725. https://doi.org/10.1002/ep.13725

Tawfik A, Ni SQ, Awad HM, Ismail S, Tyagi VK, Khan MS, Qyyum MA, Lee, M. Recent approaches for the production of high value-added biofuels from gelatinous wastewater. Energies, 2021 Aug;14(16):4936. https://doi.org/10.3390/en14164936

Wang G, Yu N, Guo Y. A novel process to recycle the highly concentrated calcium and chloride ions in the gelatin acidification wastewater. J Cleaner Prod. 2018 Jul;188:62–68. https://doi.org/10.1016/j.jclepro.2018.03.215

Wang J, Chen C. Chitosan-based biosorbents: Modification and application for biosorption of heavy metals and radionuclides. Bioresour Technol. 2014 May;160:129–141. https://doi.org/10.1016/j.biortech.2013.12.110

Wang JP, Liu B, Liu GH, Chen DJ, Zhu YJ, Chen Z, Che JM. Genome sequence of *Virgibacillus pantothenticus* DSM 26T (ATCC 14576), a mesophilic and halotolerant bacterium isolated from soil. Genome Announc. 2015 Sep;3(5):e01064-15. https://doi.org/10.1128/genomeA.01064-15

Wang XL, Li Y, Huang J, Zhou YZ, Li BL, Liu DB. Efficiency and mechanism of adsorption of low concentration uranium in water by extracellular polymeric substances. J Environ Radioact. 2019 Feb; 197:81–89. https://doi.org/10.1016/j.jenvrad.2018.12.002

Xu C, Wang J, Yang T, Chen X, Liu X, Ding X. Adsorption of uranium by amidoximated chitosan-grafted polyacrylonitrile, using response surface methodology. Carbohydr Polym. 2015 May; 121:79–85. https://doi.org/10.1016/j.carbpol.2014.12.024

Xu X, Zhang Z, Huang Q, Chen W. Biosorption performance of multimetal resistant fungus *Penicillium chrysogenum* XJ-1 for removal of Cu^{2+} and Cr^{6+} from aqueous solutions. Geomicrobiol J. 2017;35(1):40–49. https://doi.org/10.1080/01490451.2017.1310331

Yang Y, Hu M, Zhou D, Fan W, Wang X, Huo M. Bioremoval of Cu^{2+} from CMP wastewater by a novel copper-resistant bacterium *Cupriavidus gilardii* CR3: Characteristics and mechanisms. RSC Adv. 2017;7:18793–18802. https://doi.org/10.1039/c7ra01163f

Yuan W, Cheng J, Huang H, Xiong S, Gao J, Zhang J, Feng S. Optimization of cadmium biosorption by *Shewanella putrefaciens* using a Box-Behnken design. Ecotoxicol Environ Saf. 2019 Jul;175:138–147. https://doi.org/10.1016/j.ecoenv.2019.03.057